DOI:
10.1016/j.jcmg.2020.01.006

Coronary Magnetic Resonance Angiography – Technical Innovations Leading us to the Promised Land?

Reza Hajhosseiny MD[1,2], Aurelien Bustin PhD[1], Camila Munoz PhD[1], Imran Rashid MD[1], Gastao Cruz MD[1], Warren J. Manning MD[3], Claudia Prieto PhD[1,4] and René M. Botnar PhD[1,4]

1. School of Biomedical Engineering and Imaging Sciences, King's College London, London, United Kingdom
2. National Heart and Lung Institute, Imperial College London, London, United Kingdom
3. Department of Medicine (Cardiovascular Division) and Radiology, Beth Israel Deaconess Medical Center and Harvard Medical School, Boston, Massachusetts, USA
4. Escuela de Ingeniería, Pontificia Universidad Catolica de Chile, Santiago, Chile

Address for correspondence:
Dr Reza Hajhosseiny
School of Biomedical Engineering and Imaging Sciences
King's College London
3rd floor Lambeth Wing
London, SE1 7EH
United Kingdom
Email: reza.hajhosseiny@kcl.ac.uk
Telephone: +44 020 7188 7188
Twitter handle: @KCL_CardiacMR

Conflict of Interest: None

Financial Disclosures: None

Abstract

Coronary artery disease remains the leading cause of cardiovascular morbidity and mortality. Invasive X-ray angiography and coronary computed tomography angiography are established gold standards for coronary luminography. However, they expose patients to invasive complications, ionizing radiation and iodinated contrast agents. Amongst a number of imaging modalities, coronary cardiovascular magnetic resonance (CMR) angiography may be used in some cases as an alternative for the detection and monitoring of coronary arterial stenosis, with advantages including its versatility, excellent soft tissue characterization, and avoidance of ionizing radiation and iodinated contrast agents. In this review, we will explore the recent advances in motion correction, image acceleration and reconstruction technologies that are bringing coronary CMR angiography closer to widespread clinical implementation.

Abbreviations:

BOOST - Bright-blood and black-blOOd phase SensiTive
CAD – Coronary Artery Disease
CATCH - Coronary Atherosclerosis T1-weighed Characterization with integrated anatomical reference
CHIP – Coronary high intensity plaque
CMR – Cardiovascular Magnetic Resonance
CTA – Computed Tomography Angiography
FFR – Fractional Flow Reserve
FFR-CT - Fractional Flow Reserve Computed Tomography
IFR – Instantaneous Wave-Free Ratio
iNAV – Image Navigator
LGE – Late Gadolinium Enhancement
PSIR – Phase Sensitive Inversion Recovery

Keywords: Coronary Angiography, Magnetic Resonance Imaging, Atherosclerosis, CMR, CAD

Highlights:

- Invasive X-ray angiography and coronary computed tomography angiography are established gold standards for coronary angiography.
- Coronary CMR angiography could provide a safe, non-invasive, radiation and iodinated contrast free alternative.
- Technological innovations including advanced motion correction, image acceleration and reconstruction techniques have transformed the field of coronary CMR angiography.
- Multicenter clinical trials implementing these technological advances are needed to validate the improvements needed for more widespread clinical use.

1.0. Introduction

Cardiovascular disease is the leading cause of mortality worldwide, with expected direct and indirect costs of $1.1 trillion by 2035 in the United States alone(1). Atherosclerotic coronary artery disease (CAD) is the main contributor to cardiovascular disease (44%)(1)(2)(3). The early detection of CAD enables targeted risk stratification and prophylactic treatment of patients most at risk of developing ischemic cardiovascular disease. In recent years, cardiovascular magnetic resonance (CMR) has emerged as a safe, non-invasive, radiation and iodinated contrast free alternative for imaging of coronary artery stenosis. In a seminal multicenter study of 109 patients comparing non-contrast coronary CMR angiography vs. X-ray angiography, the sensitivity, specificity, positive and negative predictive values, and accuracy of CMR were 93%, 42%, 70%, 81%, and 72% respectively; indicating the potential of CMR to exclude significant CAD (Table 1)(4). In a similar study of 127 patients, the sensitivity, specificity, positive and negative predictive values, and accuracy of CMR were 88%, 72%, 71%, 88%, and 79% respectively (Table 1)(5). In a further study of 207 patients with suspected CAD who underwent non-contrast whole-heart coronary CMR angiography, coronary stenosis (≥50% diameter reduction) were significantly associated with adverse cardiac events (cardiac death, myocardial infarction, and unstable angina) and all cardiac events (including revascularization >90 days after CMR) (Table 1)(6). However, widespread clinical implementation is currently hampered by long acquisition times, cumbersome scan planning, low spatial-resolution and motion related image quality degradation.

In this review, we summarize the established imaging modalities for coronary artery imaging, before focusing on the latest advances in CMR technology, which are overcoming the challenges facing coronary CMR angiography.

2.0. Established coronary artery imaging technologies

2.1. Invasive X-ray coronary angiography

Quantitative invasive X-ray coronary angiography is the clinical gold standard imaging modality for the assessment of CAD. With a spatial resolution of up to 0.1 mm, it is unrivalled in the assessment of distal coronary anatomy. The added advantage of ad-hoc percutaneous coronary intervention (PCI) is undisputed in the acute setting, providing convenience and cost effectiveness. In patients with symptomatic but stable CAD, invasive assessment of coronary physiology and functionally guided PCI with fractional flow reserve (FFR) or instantaneous wave-free ratio (IFR) pressure wiring has been shown to be prognostically significant and are now the established gold-standard approach to revascularization in stable CAD (7)(8).

However, invasive complications (death, stroke, myocardial and vascular injury, pain and bleeding), long term cumulative risk from ionizing radiation and short term risk of iodinated contrast mediated nephropathy limit its capacity as a screening/monitoring tool in patients with suspected/stable CAD. Finally, it provides inadequate plaque characterization, especially in the context of lumen preserving positive remodeling.

2.2. Intravascular ultrasound (IVUS) and optical coherence tomography (OCT)

Intravascular imaging (IVUS and OCT) combines angiography with real time information on coronary vessel wall and plaque composition (lipid core, thrombus, hemorrhage, fibrous tissue, calcium and thin cap fibro-atheroma) (9)(10). They are unparalleled in PCI planning (sizing of coronary lumen and stent positioning, post stent deployment optimization, assessment of pre and post intervention coronary dissection) (9).

However, invasive complications remain a risk and while OCT has a 10-fold higher spatial resolution (up to 0.01 mm) compared to IVUS (0.1 – 0.15 mm) (11), in clinical practice it is largely reliant on iodinated contrast agents (although dextran or saline are emerging as viable alternatives) (9)(10). Therefore, clinical guidelines recommend their use as ad-hoc to invasive X-ray coronary angiography (9)(10).

2.3. Coronary computed tomography angiography (CTA)

The evolution of coronary computed tomography angiography (CTA) has been remarkable, in large part due to technical advancements in X-ray tubes, faster gantry rotation, multiple parallel detector rings and related decreased slice thickness (12). With a spatial resolution as low as 0.4 mm, negative predictive value in the high 90%s, non-invasive nature and relatively low cost compared to invasive coronary angiography, it is recommended in clinical guidelines as the imaging modality of choice in patients with stable symptoms at low-intermediate risk of CAD (12)(13)(14). Further technological advances enable functional fractional flow reserve assessment (FFR-CT) and plaque assessment (overall plaque burden, spotty calcification, plaque attenuation pattern and positive remodeling index) (12)(13)(14).

However, coronary CTA is limited by ionizing radiation and the need for iodinated contrast, while blooming artefact from extensive coronary calcification hampers the accurate assessment of stenosis. In addition, patients with renal impairment, resistant tachycardia/arrhythmias, hypersensitivity to iodinated contrast agents, pregnancy, and inability to follow breath-hold instructions are ongoing challenges (15).

3.0. Coronary (CMR) angiography

Given these limitations, there is a clear need for an alternative modality for the early detection and long-term monitoring of CAD. Over the past two decades, CMR technology has leaped, potentially enabling a safe, versatile, non-invasive, radiation and iodinated contrast free alternative for coronary angiography.

CMR is the clinical gold-standard modality for the assessment of cardiac structure, volume, function, tissue characterization and myocardial perfusion (16). Lagging behind is coronary CMR angiography. Reasons for this include lower spatial resolution compared to coronary CTA (1 mm vs. 0.4 - 0.6 mm), significantly longer acquisition time, higher cost, more complex scan planning, and image quality degradation due to cardiac, respiratory and patient motion; all resulting in lower sensitivity and specificity compared to coronary CTA (16). As a result, coronary CMR angiography is clinically limited to suspected anomalous coronary arteries, coronary artery aneurysms (e.g. Kawasaki's disease) and assessment of the proximal coronary arteries (Figures 1 and 2)(16)(17).

However, innovations in CMR technology (including image acceleration, motion correction, reconstruction frameworks, simplified scan planning, higher field strength, use of gadolinium-based contrast agents and nitrates) are overcoming these challenges. Furthermore, CMR plaque characterization is gaining significant research interest for early detection and treatment of atherosclerosis.

3.1. Field strength, contrast agents and use of nitrates

At higher magnetic field strength (e.g. 3T), the signal to noise ratio (SNR) is increased, helped by gradient echo sequences, which are less susceptible to magnetic field inhomogeneities and the need for lower flip angles to achieve sufficient blood contrast (17).

Contrast agents shorten the T1 relaxation of the coronary artery blood pool and help improve SNR and image quality compared with 1.5T (18)(19)(20), enabling a spatial resolution of up to 0.35 mm (21), albeit at an increased acquisition time of up to 9 mins. CMR blood-pool agents that do not extravasate (e.g. gadofoveset) have a greater T1 shortening effect compared to extracellular agents (e.g. gadobenate dimeglumine), providing marginally better performance for coronary CMR angiography at 3T (20)(22)(23)(24)(25).

Nitrates are coronary vasodilators that act by relaxing vascular smooth muscle and are frequently used in both invasive X-ray coronary angiography and coronary CTA to improve image quality and diagnostic performance. However, use of nitrates in coronary CMR angiography is not well established. In a study of 25 healthy subjects undergoing three-dimensional (3D) coronary CMR angiography, sublingual nitrates significantly improved coronary vessel sharpness, image quality score and maximum SNR(26). In a separate study of 15 healthy subjects undergoing 3D free-breathing coronary CMR angiography, luminal diameter was significantly larger with sublingual nitrates, although there was no significant difference in terms of SNR and overall image quality scores (27). Further clinical validation studies using both nitrates and beta-blockers with coronary CMR angiography are needed to provide a fair comparison with coronary CTA.

3.2. CMR motion correction techniques

The major challenges that need to be overcome in coronary CMR angiography are: 1) image quality degradation due to cardiac and respiratory motion, 2) suboptimal spatial resolution to facilitate clinically feasible acquisition times and 3) complex diaphragmatic navigator planning. Current strategies to deal with cardiac and respiratory motion and scan planning as

well as the use of novel undersampled reconstruction techniques to enable shorter scan times are discussed hereafter.

3.2.1. Cardiac motion correction

As with coronary CTA, motion artefacts from cardiac contraction and relaxation are minimized by using prospective electrocardiographic (ECG) gating to acquire data during the quiescent phase of the cardiac cycle, usually in mid-to-late diastole. However, this approach is disadvantaged by cardiac arrhythmias and variable heart rates as the onset and duration of the ideal acquisition window is heart rate dependent. While it is possible to acquire data during systole, which is less sensitive to arrhythmias, the quiescent period is relatively short, resulting in longer acquisition times (more heart beats). An alternative approach is to continuously acquire data in a similar manner to coronary CTA and to then retrospectively reconstruct multiple cardiac phases and select the phase with the least motion artefacts, thereby minimizing user input during planning (28)(29).

3.2.2. Respiratory motion correction

Advances in respiratory motion correction is spearheading the renaissance of coronary CMR angiography. Initial CMR sequences utilized breath-holding to suppress respiratory motion artefacts and to improve image quality (30)(31)(32)(33). These sequences employed two-dimensional (2D) encoding and therefore provided limited coverage of the coronary arteries. Further advances in image acceleration subsequently enabled 3D coronary CMR angiography data acquisitions within a single breath-hold (34)(35)(36), but image quality was often suboptimal due to cranial diaphragmatic drift and limited patient ability to perform and sustain a long breath-hold (37)(38). Therefore, attention shifted to free-breathing motion compensated 3D coronary CMR angiography (37)(39).

3.2.2.1. Respiratory gating

External respiratory monitoring devices such as respiratory bellows (40), amplitude demodulation of the ECG signal (41), and ultra-wideband sensors (42) allow the coding of the patient's respiratory phase into inspiration and expiration with high accuracy and temporal-resolution. This allows image data to only be acquired at end expiration, when respiratory motion is minimal/absent (respiratory gating). However, this approach is unable to quantify in detail the extent and 3D nature of respiratory motion (superior-inferior, right-left, anterior-posterior, rotation). It is also highly inefficient as data is acquired only at end expiration, making the scans time consuming and expensive. Attaching the devices to patients further prolongs the scanning process.

In an alternative approach, respiratory navigators incorporate the CMR signal to estimate the respiratory displacement of the heart. The diaphragmatic 1D navigator (d1D NAV) (43)(44) exploits the good delineation of the liver-diaphragm interface to enable superior-inferior respiratory translational motion estimation both for gating and/or correction. However, there is a non-linear relationship (45) between the displacement of the diaphragm and the heart, requiring utilization of a population averaged scaling factor of 0.6 (46)(47). Furthermore, complex diaphragmatic navigator planning, prolonged and unpredictable acquisition times due to respiratory gating remain drawbacks (37)(44).

3.2.2.3. Self navigation

The "self-navigation" (48) approach was introduced to overcome some of these disadvantages. Here, the respiratory motion of the heart is estimated directly from the acquired CMR data (48)(49) thereby avoiding the correction factor, relaxing the need for

respiratory gating and enabling 1D translational respiratory motion correction (50). This approach has been used to enable 100% respiratory scan efficiency, using data acquired at every point of the respiratory cycle in the reconstruction process (51)(52)(53).

In a clinical validation study, 78 patients referred for CMR were examined with 3D 1.5T self-navigated contrast-enhanced coronary CMR angiography at 1.15 mm isotropic spatial-resolution, with an average scan time of 7.4 minutes (54) (Table 1). The main/proximal, middle and distal coronary artery segments could be visualized in 92%, 84%, and 56% of cases respectively, with significantly higher vessel sharpness in the proximal segments ($p<0.05$). Per vessel sensitivity and specificity for stenosis detection were 65% and 85%, compared with invasive X-ray coronary angiography (Figure 3).

A disadvantage of self-navigation is the difficulty in separating moving (e.g. heart) from static (e.g. chest wall) tissue, which reduces the motion correction performance(55).

3.2.2.4. Image navigators (iNAVs)

The principle behind image-based navigators (iNAVs) is to separate moving tissue from static tissue by obtaining a 2D/3D low spatial resolution image/volume at every heartbeat prior to the high resolution CMR acquisition (55)(56)(57)(58)(59). One advantage of this technique is that respiratory motion can be estimated in several directions to account for the complex motion of the heart (some of these are outlined below). Furthermore, it does not require additional planning as it can be prescribed with the same field of view (FOV) and orientation as the high-resolution 3D coronary CMR sequence. Moreover, iNAV approaches allow for 100% respiratory scan efficiency, predictable and faster scan time.

In a study of 29 patients with congenital heart disease, Henningsson et al (60) combined the iNAV with respiratory bellows in a 3D whole-heart coronary CMR sequence. Compared to the d1D NAV, the iNAV scan time was significantly shorter ($p<0.01$), while vessel sharpness, depiction and visual scores were significantly improved (Table 1 and Figure 4). In a further clinical validation study, 31 patients suspected of having CAD were examined with a 3D whole-heart iNAV coronary CMR sequence, yielding excellent diagnostic image quality in the proximal, middle and distal coronary segments (98%, 94% and 91%, respectively) (61) (Table 1 and Figure 5). The sensitivity, specificity, and negative predictive values were 86%, 83%, and 95% per patient, 80%, 92%, and 97% per vessel and 73%, 95%, and 98% per segment; compared with invasive X-ray coronary angiography.

3.3. Acceleration and reconstruction techniques in coronary CMR angiography

3.3.1. Recap of undersampling techniques in CMR

Despite advances in CMR technology outlined above, a fully sampled whole-heart 3D coronary CMR angiography acquisition with 1 mm isotropic resolution can take up to 30 minutes, even with 100% respiratory scan efficiency (62). This is not practical in the clinical setting and therefore further image acceleration techniques are required. Undersampled reconstruction techniques have been proposed to accelerate the scan by collecting less data than required by the Nyquist theorem and using assumptions and prior information to recover the non-acquired data, thus maintaining image quality. Undersampled reconstruction techniques employed in CMR include partial Fourier, parallel imaging, and compressed sensing.

Partial Fourier exploits the symmetry of k-space data, and only a fraction (typically >60%) of data are acquired with the full image subsequently reconstructed with homodyne reconstruction (63). Parallel imaging takes advantage of the spatial information inherent in phased-array radio-frequency coils to provide additional spatial information that can be used to recover the non-acquired data, reducing image acquisition time (64)(65)(66). Compressed sensing exploits the assumption that the image to be reconstructed has a sparse representation in a given domain, which combined with pseudo-random undersampling and non-linear reconstruction enables highly accelerated acquisitions (67).

3.3.2. Novel 3D coronary CMR angiography sequences and reconstructions

Several 3D high-resolution whole-heart coronary CMR angiography sequences have been proposed which incorporate a combination of the principles outlined above. For technical details, please refer to the original manuscripts. In 2011, Bhat et al (68) proposed a novel non-contrast approach at 1.5T whereby 3D radial trajectory k-space undersampled data acquisition was combined with the d1D NAV to assign the acquired data into "respiratory bins" (specific phases in the respiratory cycle). Registration algorithms were then used to estimate the motion between each bin and a reference end-expiratory bin. Images from all respiratory bins were then motion corrected to the common respiratory position and averaged to produce a respiratory motion corrected image. This approach allowed 100% scan efficiency with a significantly shorter acquisition time compared to d1D NAV respiratory gating (6.8 ± 0.9 vs. 16.2 ± 2.8 min, $p<0.001$), with similar image quality (Table 1). Drawbacks include prolonged scan planning due to diaphragmatic navigator positioning, lower SNR of radial sampling, and prolonged reconstruction time if compressed sensing is used.

To overcome the prolonged scan planning, this approach was extended to self-navigation (29)(48)(49), producing similar image quality compared to d1D NAV gating and d1D NAV-binning models. To improve the lower SNR and shorten reconstruction times of radial sampling, we (69) proposed a fully sampled golden-step Cartesian trajectory for 3D coronary CMR angiography. This approach was combined with 2D iNAVs (55), which are used to estimate beat-to-beat 2D translational respiratory motion of the heart and to assign the acquired 3D data to different respiratory bins. Using this binned data, 3D non-rigid respiratory motion can be estimated and motion-corrected images can be reconstructed by combining beat-to-beat 2D translational and bin-to-bin 3D non-rigid motion correction of the binned data to a common reference position. (Table 1 and Figure 6)(70). Building on a highly undersampled patch-based CMR reconstruction framework(71), Bustin et al (62) combined 2D translational respiratory motion correction with a highly undersampled Cartesian trajectory, and proposed a novel 3D patch-based low-rank reconstruction, enabling sub-mm (0.9 mm) isotropic spatial-resolution free-breathing whole-heart 3D CMR angiography with 5-7 minutes acquisition time and ~3 minutes reconstruction time (62). The overall image quality was at least equivalent to the fully sampled sequence and superior to both parallel imaging and compressed sensing reconstruction methods (Table 1 and Figure 7). This approach has been extended to also incorporate bin-to-bin non-rigid respiratory motion correction and has been compared against coronary CTA in patients with suspected CAD, holding promise for the detection and exclusion of significant coronary artery stenosis (72)(73). The final results of this clinical study are awaited.

Respiratory resolved reconstruction frameworks have also been introduced to account for the complex non-rigid 3D motion of the heart. XD-GRASP (eXtra-Dimensional Golden-angle RAdial Sparse Parallel MRI) combined with a spiral phyllotaxis 3D radial trajectory enables

respiratory resolved 3D coronary CMR angiography. This approach was evaluated in healthy subjects and patients (74), showing significant improvement in vessel length and sharpness compared to 1D respiratory self-navigation reconstruction (Table 1 and Figure 9). This approach was extended to also reconstruct cardiac phases (5D whole-heart) from so called "free-running" acquisitions (Figure 8) (28)(75)(76)(77). Drawbacks of this approach include longer reconstruction times and lower SNR compared to Cartesian sampling (78)(79). In order to enable motion resolved Cartesian coronary CMR angiography, XD-ORCCA (Optimized Respiratory-resolved Cartesian Coronary MR Angiography) has been proposed (78), which exploits the 2D iNAV to both correct for intra-bin respiratory motion (superior-inferior and left-right) and to increase sparsity by aligning all bins with the end-expiratory bin. Compared to XD-GRASP, coronary vessel length and sharpness was significantly improved with XD-ORCCA, independent of breathing pattern (Table 1 and Figure 10) (78).

4.0. Coronary CMR plaque imaging

For a detailed discussion on coronary CMR plaque imaging, please refer to the recent articles (80)(81)(82)(83)(84). Coronary CMR imaging can identify high-risk coronary plaques by exploiting the T1 shortening effects of plaque features (intraplaque hemorrhage, thrombus, lipid core, thin-cap fibroatheroma, calcification, macrophages, and cholesterol clusters), with or without exogenous contrast agents (85)(86)(87)(88)(89). CMR identification of high-risk plaque is prognostically significant, independent of coronary luminal stenosis (90). However, widespread clinical translation is limited by similar technical challenges to coronary CMR angiography, including respiratory motion artefacts, prolonged and unpredictable scan times as well as misalignment between coronary CMR angiography and plaque imaging as data are acquired sequentially. To overcome some of these limitations, Xie et al. proposed a framework (so called CATCH) which combines advanced motion correction techniques to

enable simultaneous multi contrast bright and black blood coronary artery angiography and visualization of high intensity coronary plaque (Figure 11) (91)(92). However, as the respiratory motion parameters are partially shared among the bright-blood and black-blood datasets, coronary plaque-misregistration may not be avoided. To overcome this, Ginami et al. (93)(94) introduced the 3D whole-heart non-contrast enhanced Bright-blood and black-blOOd phase SensiTive (BOOST) inversion recovery sequence for simultaneous coronary angiography and thrombus/intraplaque hemorrhage visualization. This is achieved by alternating the acquisition of two different bright-blood datasets, which are then combined in a phase-sensitive inversion recovery (PSIR)-like reconstruction to obtain a third, black-blood dataset. The two differently weighted bright-blood datasets enable coronary angiography and allow respiratory motion to be independently estimated/corrected, further reducing the probability of misregistration artefacts. The co-registered black-blood PSIR dataset potentially enables thrombus/intraplaque hemorrhage visualization (Figure 12).

5.0. CMR myocardial viability and functional assessment

A detailed discussion on CMR myocardial scar and functional assessment is beyond the scope of this article. Briefly, unless a significant stenosis affects the left main stem, coronary revascularization should be guided by comprehensive functional assessment (95)(96). CMR has the unique ability to assess the transmural extent of infarction scar within each myocardial segment, empowering clinicians to more accurately select patients most suitable for coronary revascularization (97). Furthermore, large multi-center clinical studies have proven the ability of CMR to reliably and accurately assess myocardial ischemia, compared against nuclear perfusion and FFR as the non-invasive and invasive gold-standards respectively (98)(99)(100). Incorporating anatomical coronary information to these features

could potentially promote CMR as the most complete single imaging modality for CAD evaluation.

6.0. Conclusion and future directions

Despite the impressive progress in coronary CMR angiography technology, these sequences are largely adopted by academic research centers. Multicenter clinical validation and prognosis trials with the use of beta-blockers and nitrates similar to coronary CTA and protocol simplifications are clearly required before coronary CMR angiography can plausibly rival invasive coronary angiogram and coronary CTA. However, the increasing availability of more powerful (3T and above) and smarter (equipped with more sensors and artificial intelligence) CMR scanners combined with the technology outlined above may herald an era of coronary CTA equivalent image quality without the need for nephrotoxic contrast agents or ionizing radiation. Further advances in single scan multi-contrast angiography and plaque characterization can prognostically supplement CMR atherosclerosis imaging. Finally, the clinical integration of coronary CMR angiography with perfusion and myocardial scar imaging could establish CMR as the most comprehensive non-invasive single imaging modality for the evaluation of CAD.

References

1. Benjamin EJ., Virani SS., Callaway CW., et al. Heart disease and stroke statistics-2018 update: A report from the American Heart Association. Circulation 2018;137(12):e67–492. Doi: 10.1161/CIR.0000000000000558.
2. Libby P. Current concepts of the pathogenesis of the acute coronary syndromes. Circulation 2001;104(3):365–72.
3. Ross R. The pathogenesis of atherosclerosis: a perspective for the 1990s. Nature 1993;362(6423):801–9. Doi: 10.1038/362801a0.
4. Kim WY., Danias PG., Stuber M., et al. Coronary magnetic resonance angiography for the detection of coronary stenoses. N Engl J Med 2001;345(26):1863–9. Doi: 10.1056/NEJMoa010866.
5. Kato S., Kitagawa K., Ishida N., et al. Assessment of coronary artery disease using magnetic resonance coronary angiography: a national multicenter trial. J Am Coll Cardiol 2010;56(12):983–91. Doi: 10.1016/j.jacc.2010.01.071.
6. Yoon YE., Kitagawa K., Kato S., et al. Prognostic value of coronary magnetic resonance angiography for prediction of cardiac events in patients with suspected coronary artery disease. J Am Coll Cardiol 2012;60(22):2316–22. Doi: 10.1016/J.JACC.2012.07.060.
7. De Bruyne B., Pijls NHJ., Kalesan B., et al. Fractional flow reserve–guided PCI versus medical therapy in stable coronary disease. N Engl J Med 2012;367(11):991–1001. Doi: 10.1056/nejmoa1205361.
8. Götberg M., Christiansen EH., Gudmundsdottir IJ., et al. Instantaneous wave-free ratio versus fractional flow reserve to guide PCI. N Engl J Med 2017;376(19):1813–23. Doi: 10.1056/NEJMoa1616540.
9. Rathod KS., Hamshere SM., Jones DA., Mathur A. Intravascular ultrasound versus

optical coherence tomography for coronary artery imaging – apples and oranges? Interv Cardiol Rev 2015;10(1):8. Doi: 10.15420/icr.2015.10.1.8.

10. Tian J., Dauerman H., Toma C., et al. Prevalence and characteristics of TCFA and degree of coronary artery stenosis. J Am Coll Cardiol 2014;64(7):672–80. Doi: 10.1016/j.jacc.2014.05.052.
11. Popescu DP., Choo-Smith L-P., Flueraru C., et al. Optical coherence tomography: fundamental principles, instrumental designs and biomedical applications. Biophys Rev 2011;3(3):155. Doi: 10.1007/s12551-011-0054-7.
12. Kolossváry M., Szilveszter B., Merkely B., Maurovich-Horvat P. Plaque imaging with CT-a comprehensive review on coronary CT angiography based risk assessment. Cardiovasc Diagn Ther 2017;7(5):489–506. Doi: 10.21037/cdt.2016.11.06.
13. Alfakih K., Byrne J., Monaghan M. CT coronary angiography: a paradigm shift for functional imaging tests. Open Hear 2018;5(1):e000754. Doi: 10.1136/openhrt-2017-000754.
14. Doris MK., Newby DE. How should CT coronary angiography be integrated into the management of patients with chest pain and how does this affect outcomes? Eur Hear J - Qual Care Clin Outcomes 2016;2(2):72–80. Doi: 10.1093/ehjqcco/qcv027.
15. Abbara S., Blanke P., Maroules CD., et al. Guidelines SCCT guidelines for the performance and acquisition of coronary computed tomographic angiography: A report of the Society of Cardiovascular Computed Tomography Guidelines Committee Endorsed by the North American Society for Cardiovascular Imaging (NASCI). J Cardiovasc Comput Tomogr 2016;10:435–49. Doi: 10.1016/j.jcct.2016.10.002.
16. Mangla A., Oliveros E., Williams KA., Kalra DK. Cardiac imaging in the diagnosis of coronary artery disease. Curr Probl Cardiol 2017;42(10):316–66. Doi: 10.1016/J.CPCARDIOL.2017.04.005.

17. Hamdy A., Ishida M., Sakuma H. Cardiac MR assessment of coronary arteries. CVIA 2017;1(1):49–59. Doi: 10.22468/cvia.2016.00066.

18. Prompona M., Cyran C., Nikolaou K., Bauner K., Reiser M., Huber A. Contrast-enhanced whole-heart coronary MRA using gadofosveset: 3.0 T versus 1.5 T. Acad Radiol 2010;17(7):862–70. Doi: 10.1016/J.ACRA.2010.02.009.

19. Stuber M., Botnar RM., Fischer SE., et al. Preliminary report on in vivo coronary MRA at 3 Tesla in humans. Magn Reson Med 2002;48(3):425–9. Doi: 10.1002/mrm.10240.

20. Raman FS., Nacif MS., Cater G., et al. 3.0-T whole-heart coronary magnetic resonance angiography: Comparison of gadobenate dimeglumine and gadofosveset trisodium. Int J Cardiovasc Imaging 2013;29(5):1085–94. Doi: 10.1007/s10554-013-0192-z.

21. Gharib AM., Abd-Elmoniem KZ., Ho VB., et al. The feasibility of 350 μm spatial resolution coronary magnetic resonance angiography at 3 T in humans. Invest Radiol 2012;47(6):339–45. Doi: 10.1097/RLI.0b013e3182479ec4.

22. Stuber M., Botnar RM., Danias PG., et al. Contrast agent-enhanced, free-breathing, three-dimensional coronary magnetic resonance angiography. J Magn Reson Imaging 1999;10(5):790–9. Doi: 10.1002/(SICI)1522-2586(199911)10:5<790::AID-JMRI25>3.0.CO;2-I.

23. Paetsch I., Jahnke C., Barkhausen J., et al. Detection of coronary stenoses with contrast enhanced, three-dimensional free breathing coronary MR angiography using the gadolinium-based intravascular contrast agent gadocoletic acid (B-22956). J Cardiovasc Magn Reson 2006;8(3):509–16. Doi: 10.1080/10976640600604922.

24. Paetsch I., Huber ME., Bornstedt A., et al. Improved three-dimensional free-breathing coronary magnetic resonance angiography using gadocoletic acid (B-22956) for intravascular contrast enhancement. J Magn Reson Imaging 2004;20(2):288–93. Doi:

10.1002/jmri.20099.

25. Kelle S., Thouet T., Tangcharoen T., et al. Whole-heart coronary magnetic resonance angiography with MS-325 (Gadofosveset). Med Sci Monit 2007;13(11):CR469-474.

26. Hu P., Chuang ML., Ngo LH., et al. Coronary MR imaging: effect of timing and dose of isosorbide dinitrate administration. Radiology 2010;254(2):401–9. Doi: 10.1148/radiol.09090483.

27. Jin H., Zeng M-S., Ge M-Y., et al. Influence of applying nitroglycerin in whole-heart free-breathing 3D coronary MR angiography. Am J Roentgenol 2010;194(4):927–32. Doi: 10.2214/AJR.09.3330.

28. Coppo S., Piccini D., Bonanno G., et al. Free-running 4D whole-heart self-navigated golden angle MRI: Initial results. Magn Reson Med 2015;74(5):1306–16. Doi: 10.1002/mrm.25523.

29. Pang J., Bhat H., Sharif B., et al. Whole-heart coronary MRA with 100% respiratory gating efficiency: Self-navigated three-dimensional retrospective image-based motion correction (TRIM). Magn Reson Med 2014;71(1):67–74. Doi: 10.1002/mrm.24628.

30. Atkinson DJ., Edelman RR. Cineangiography of the heart in a single breath hold with a segmented turboFLASH sequence. Radiology 1991;178(2):357–60. Doi: 10.1148/radiology.178.2.1987592.

31. Edelman RR., Manning WJ., Burstein D., Paulin S. Coronary arteries: breath-hold MR angiography. Radiology 1991;181(3):641–3. Doi: 10.1148/radiology.181.3.1947074.

32. Meyer CH., Hu BS., Nishimura DG., Macovski A. Fast spiral coronary artery imaging. Magn Reson Med 1992;28(2):202–13.

33. Manning WJ., Li W., Edelman RR. A preliminary report comparing magnetic resonance coronary angiography with conventional angiography. N Engl J Med 1993;328(12):828–32. Doi: 10.1056/NEJM199303253281202.

34. Wielopolski PA., van Geuns RJ., de Feyter PJ., Oudkerk M. Breath-hold coronary MR angiography with volume-targeted imaging. Radiology 1998;209(1):209–19. Doi: 10.1148/radiology.209.1.9769834.

35. Li D., Carr JC., Shea SM., et al. Coronary arteries: magnetization-prepared contrast-enhanced three-dimensional volume-targeted breath-hold MR angiography. Radiology 2001;219(1):270–7. Doi: 10.1148/radiology.219.1.r01ap37270.

36. Niendorf T., Hardy CJ., Giaquinto RO., et al. Toward single breath-hold whole-heart coverage coronary MRA using highly accelerated parallel imaging with a 32-channel MR system. Magn Reson Med 2006;56(1):167–76. Doi: 10.1002/mrm.20923.

37. Li D., Kaushikkar S., Haacke EM., et al. Coronary arteries: three-dimensional MR imaging with retrospective respiratory gating. Radiology 1996;201(3):857–63. Doi: 10.1148/radiology.201.3.8939242.

38. Danias PG., Stuber M., Botnar RM., Kissinger K V., Chuang ML., Manning WJ. Navigator assessment of breath-hold duration: impact of supplemental oxygen and hyperventilation. Am J Roentgenol 1998;171(2):395–7. Doi: 10.2214/ajr.171.2.9694460.

39. Botnar RM., Stuber M., Danias PG., Kissinger K V., Manning WJ. Improved coronary artery definition with T2-weighted, free-breathing, three-dimensional coronary MRA. Circulation 1999;99(24):3139–48. Doi: 10.1161/01.cir.99.24.3139.

40. Runge VM., Clanton JA., Partain CL., James AE. Respiratory gating in magnetic resonance imaging at 0.5 Tesla. Radiology 1984;151(2):521–3. Doi: 10.1148/radiology.151.2.6709928.

41. Felblinger J., Boesch C. Amplitude demodulation of the electrocardiogram signal (ECG) for respiration monitoring and compensation during MR examinations. Magn Reson Med 1997;38(1):129–36.

42. Thiel F., Kosch O., Seifert F. Ultra-wideband sensors for improved magnetic resonance imaging, cardiovascular monitoring and tumour diagnostics. Sensors 2010;10(12):10778–802. Doi: 10.3390/s101210778.

43. Ehman RL., Felmlee JP. Adaptive technique for high-definition MR imaging of moving structures. Radiology 1989;173(1):255–63. Doi: 10.1148/radiology.173.1.2781017.

44. McConnell M V., Khasgiwala VC., Savord BJ., et al. Comparison of respiratory suppression methods and navigator locations for MR coronary angiography. Am J Roentgenol 1997;168(5):1369–75. Doi: 10.2214/ajr.168.5.9129447.

45. Nehrke K., Börnert P., Manke D., Böck JC. Free-breathing cardiac MR imaging: study of implications of respiratory motion—initial results. Radiology 2001;220(3):810–5. Doi: 10.1148/radiol.2203010132.

46. Wang Y., Riederer SJ., Ehman RL. Respiratory motion of the heart: kinematics and the implications for the spatial resolution in coronary imaging. Magn Reson Med 1995;33(5):713–9.

47. Nagel E., Bornstedt A., Schnackenburg B., Hug J., Oswald H., Fleck E. Optimization of realtime adaptive navigator correction for 3D magnetic resonance coronary angiography. Magn Reson Med 1999;42(2):408–11.

48. Stehning C., Börnert P., Nehrke K., Eggers H., Stuber M. Free-breathing whole-heart coronary MRA with 3D radial SSFP and self-navigated image reconstruction. Magn Reson Med 2005;54(2):476–80. Doi: 10.1002/mrm.20557.

49. Piccini D., Littmann A., Nielles-Vallespin S., Zenge MO. Respiratory self-navigation for whole-heart bright-blood coronary MRI: Methods for robust isolation and automatic segmentation of the blood pool. Magn Reson Med 2012;68(2):571–9. Doi: 10.1002/mrm.23247.

50. Lai P., Bi X., Jerecic R., Li D. A respiratory self-gating technique with 3D-translation compensation for free-breathing whole-heart coronary MRA. Magn Reson Med 2009;62(3):731–8. Doi: 10.1002/mrm.22058.

51. Jhooti P., Gatehouse PD., Keegan J., Bunce NH., Taylor AM., Firmin DN. Phase ordering with automatic window selection (PAWS): A novel motion- resistant technique for 3D coronary imaging. Magn Reson Med 2000;43(3):470–80. Doi: 10.1002/(SICI)1522-2594(200003)43:3<470::AID-MRM20>3.0.CO;2-U.

52. Keegan J., Jhooti P., Babu-Narayan S V., Drivas P., Ernst S., Firmin DN. Improved respiratory efficiency of 3D late gadolinium enhancement imaging using the continuously adaptive windowing strategy (CLAWS). Magn Reson Med 2014;71(3):1064–74. Doi: 10.1002/mrm.24758.

53. Jhooti P., Wiesmann F., Taylor AM., et al. Hybrid ordered phase encoding (HOPE): an improved approach for respiratory artifact reduction. J Magn Reson Imaging n.d.;8(4):968–80.

54. Piccini D., Monney P., Sierro C., et al. Respiratory self-navigated postcontrast whole-heart coronary MR angiography: initial experience in patients. Radiology 2014;270(2):378–86. Doi: 10.1148/radiol.13132045.

55. Henningsson M., Koken P., Stehning C., Razavi R., Prieto C., Botnar RM. Whole-heart coronary MR angiography with 2D self-navigated image reconstruction. Magn Reson Med 2012;67(2):437–45. Doi: 10.1002/mrm.23027.

56. Kawaji K., Spincemaille P., Nguyen TD., et al. Direct coronary motion extraction from a 2D fat image navigator for prospectively gated coronary MR angiography. Magn Reson Med 2014;71(2):599–607. Doi: 10.1002/mrm.24698.

57. Scott AD., Keegan J., Firmin DN. Beat-to-beat respiratory motion correction with near 100% efficiency: a quantitative assessment using high-resolution coronary artery

imaging. Magn Reson Imaging 2011;29(4):568–78. Doi: 10.1016/j.mri.2010.11.004.

58. Wu HH., Gurney PT., Hu BS., Nishimura DG., McConnell M V. Free-breathing multiphase whole-heart coronary MR angiography using image-based navigators and three-dimensional cones imaging. Magn Reson Med 2013;69(4):1083–93. Doi: 10.1002/mrm.24346.

59. Addy NO., Ingle RR., Luo J., et al. 3D image-based navigators for coronary MR angiography. Magn Reson Med 2017;77(5):1874–83. Doi: 10.1002/mrm.26269.

60. Henningsson M., Hussain T., Vieira MS., et al. Whole-heart coronary MR angiography using image-based navigation for the detection of coronary anomalies in adult patients with congenital heart disease. J Magn Reson Imaging 2016;43(4):947–55. Doi: 10.1002/jmri.25058.

61. Henningsson M., Shome J., Bratis K., Vieira MS., Nagel E., Botnar RM. Diagnostic performance of image navigated coronary CMR angiography in patients with coronary artery disease. J Cardiovasc Magn Reson 2017;19(1):68. Doi: 10.1186/s12968-017-0381-3.

62. Bustin A., Ginami G., Cruz G., et al. Five-minute whole-heart coronary MRA with sub-millimeter isotropic resolution, 100% respiratory scan efficiency, and 3D-PROST reconstruction. Magn Reson Med 2019;81(1):102–15. Doi: 10.1002/mrm.27354.

63. McGibney G., Smith MR., Nichols ST., Crawley A. Quantitative evaluation of several partial Fourier reconstruction algorithms used in MRI. Magn Reson Med 1993;30(1):51–9.

64. Sodickson DK., Manning WJ. Simultaneous acquisition of spatial harmonics (SMASH): Fast imaging with radiofrequency coil arrays. Magn Reson Med 1997;38(4):591–603.

65. Pruessmann KP., Weiger M., Scheidegger MB., Boesiger P. SENSE: sensitivity

encoding for fast MRI. Magn Reson Med 1999;42(5):952–62.

66. Glockner JF., Hu HH., Stanley DW., Angelos L., King K. Parallel MR imaging: A user's guide. RadioGraphics 2005;25(5):1279–97. Doi: 10.1148/rg.255045202.

67. Lustig M., Donoho D., Pauly JM. Sparse MRI: The application of compressed sensing for rapid MR imaging. Magn Reson Med 2007;58(6):1182–95. Doi: 10.1002/mrm.21391.

68. Bhat H., Ge L., Nielles-Vallespin S., Zuehlsdorff S., Li D. 3D radial sampling and 3D affine transform-based respiratory motion correction technique for free-breathing whole-heart coronary MRA with 100% imaging efficiency. Magn Reson Med 2011;65(5):1269–77. Doi: 10.1002/mrm.22717.

69. Prieto C., Doneva M., Usman M., et al. Highly efficient respiratory motion compensated free-breathing coronary mra using golden-step Cartesian acquisition. J Magn Reson Imaging 2015;41(3):738–46. Doi: 10.1002/jmri.24602.

70. Cruz G., Atkinson D., Henningsson M., Botnar RM., Prieto C. Highly efficient nonrigid motion-corrected 3D whole-heart coronary vessel wall imaging. Magn Reson Med 2017;77(5):1894–908. Doi: 10.1002/mrm.26274.

71. Akçakaya M., Basha TA., Goddu B., et al. Low-dimensional-structure self-learning and thresholding: regularization beyond compressed sensing for MRI reconstruction. Magn Reson Med 2011;66(3):756–67. Doi: 10.1002/mrm.22841.

72. Rashid I., Bustin A., Correia T. et al. Sub-millimeter, non-contrast 3D coronary MRA for assessment of arterial stenosis: initial clinical experience and comparison with coronary CT angiography. ISMRM 27th Annual Meeting. Montreal; 2019. p. 0976.

73. Bustin A., Correia T., Rashid I. et al. Highly accelerated 3D whole-heart isotropic sub-millimeter CMRA with non-rigid motion correction. ISMRM 27th Annual Meeting. Montreal; 2019. p. 0978.

74. Piccini D., Feng L., Bonanno G., et al. Four-dimensional respiratory motion-resolved whole heart coronary MR angiography. Magn Reson Med 2017;77(4):1473–84. Doi: 10.1002/mrm.26221.

75. Pang J., Chen Y., Fan Z., et al. High efficiency coronary MR angiography with nonrigid cardiac motion correction. Magn Reson Med 2016;76(5):1345–53. Doi: 10.1002/mrm.26332.

76. Feng L., Coppo S., Piccini D., et al. 5D whole-heart sparse MRI. Magn Reson Med 2018;79(2):826–38. Doi: 10.1002/mrm.26745.

77. Di Sopra L., Piccini D., Coppo S., Stuber M., Yerly J. An automated approach to fully self-gated free-running cardiac and respiratory motion-resolved 5D whole-heart MRI. Magn Reson Med 2019;82(6):2118–32. Doi: 10.1002/mrm.27898.

78. Correia T., Ginami G., Cruz G., et al. Optimized respiratory-resolved motion-compensated 3D Cartesian coronary MR angiography. Magn Reson Med 2018;80(6):2618–29. Doi: 10.1002/mrm.27208.

79. Feng L, Chandarana H, Zhao T, Mary B, Sodickson DK OR. Golden-angle sparse liver imaging: radial or cartesian sampling. Proc 25th Annu Meet ISMRM, Honolulu, HI, 2017:1285.

80. Xie Y., Jin H., Zeng M., Li D. Coronary artery plaque imaging. Curr Atheroscler Rep 2017;19(9):37. Doi: 10.1007/s11883-017-0672-z.

81. Doris MK., Dweck MR., Fayad ZA. The future of imaging in cardiovascular disease intervention trials: 2017 and beyond. Curr Opin Lipidol 2016;27(6):605–14. Doi: 10.1097/MOL.0000000000000350.

82. Noguchi T., Nakao K., Asaumi Y., et al. Noninvasive coronary plaque imaging. J Atheroscler Thromb 2018;25(4):281–93. Doi: 10.5551/jat.RV17019.

83. Hajhosseiny R., Bahaei TS., Prieto C., Botnar RM. Molecular and nonmolecular

magnetic resonance coronary and carotid imaging. Arterioscler Thromb Vasc Biol 2019;39(4):569–82. Doi: 10.1161/ATVBAHA.118.311754.

84. Liu W., Xie Y., Wang C., et al. Atherosclerosis T1-weighted characterization (CATCH): evaluation of the accuracy for identifying intraplaque hemorrhage with histological validation in carotid and coronary artery specimens. J Cardiovasc Magn Reson 2018;20(1):27. Doi: 10.1186/s12968-018-0447-x.

85. Matsumoto K., Ehara S., Hasegawa T., et al. Localization of coronary high-intensity signals on T1-weighted MR imaging: relation to plaque morphology and clinical severity of angina pectoris. JACC Cardiovasc Imaging 2015;8(10):1143–52. Doi: 10.1016/j.jcmg.2015.06.013.

86. Ehara S., Hasegawa T., Nakata S., et al. Hyperintense plaque identified by magnetic resonance imaging relates to intracoronary thrombus as detected by optical coherence tomography in patients with angina pectoris. Eur Hear J Cardiovasc Imaging 2012;13(5):394–9. Doi: 10.1093/ehjci/jer305.

87. Maintz D., Ozgun M., Hoffmeier A., et al. Selective coronary artery plaque visualization and differentiation by contrast-enhanced inversion prepared MRI. Eur Heart J 2006;27(14):1732–6. Doi: 10.1093/eurheartj/ehl102.

88. Yeon SB., Sabir A., Clouse M., et al. Delayed-enhancement cardiovascular magnetic resonance coronary artery wall imaging. J Am Coll Cardiol 2007;50(5):441–7. Doi: 10.1016/j.jacc.2007.03.052.

89. Ibrahim T., Makowski MR., Jankauskas A., et al. Serial contrast-enhanced cardiac magnetic resonance imaging demonstrates regression of hyperenhancement within the coronary artery wall in patients after acute myocardial infarction. JACC Cardiovasc Imaging 2009;2(5):580–8. Doi: 10.1016/j.jcmg.2008.12.029.

90. Noguchi T., Kawasaki T., Tanaka A., et al. High-intensity signals in coronary plaques

on noncontrast T1-weighted magnetic resonance imaging as a novel determinant of coronary events. J Am Coll Cardiol 2014;63(10):989–99. Doi: 10.1016/j.jacc.2013.11.034.

91. Xie Y., Pang J., Kim Y., et al. Coronary Atherosclerosis T1-weighed Characterization with integrated anatomical reference (CATCH). J Cardiovasc Magn Reson 2016;18(Suppl 1):O22. Doi: 10.1186/1532-429X-18-S1-O22.

92. Xie Y., Kim YJ., Pang J., et al. Coronary atherosclerosis T1-weighed characterization with integrated anatomical reference: comparison with high-risk plaque features detected by invasive coronary imaging. JACC Cardiovasc Imaging 2017;10(6):637–48. Doi: 10.1016/j.jcmg.2016.06.014.

93. Ginami G., Neji R., Phinikaridou A., Whitaker J., Botnar RM., Prieto C. Simultaneous bright- and black-blood whole-heart MRI for noncontrast enhanced coronary lumen and thrombus visualization. Magn Reson Med 2018;79(3):1460–72. Doi: 10.1002/mrm.26815.

94. Ginami G., Neji R., Rashid I., et al. 3D whole-heart phase sensitive inversion recovery CMR for simultaneous black-blood late gadolinium enhancement and bright-blood coronary CMR angiography. J Cardiovasc Magn Reson 2017;19(1):94. Doi: 10.1186/s12968-017-0405-z.

95. Kolh P., Windecker S., Alfonso F., et al. 2014 ESC/EACTS Guidelines on myocardial revascularization. Eur J Cardio-Thoracic Surg 2014. Doi: 10.1093/ejcts/ezu366.

96. Patel MR., White RD., Abbara S., et al. 2013 ACCF/ACR/ASE/ASNC/SCCT/SCMR appropriate utilization of cardiovascular imaging in heart failure: a joint report of the American College of Radiology Appropriateness Criteria Committee and the American College of Cardiology Foundation Appropriate Use C. J Am Coll Cardiol 2013;61(21):2207–31. Doi: 10.1016/j.jacc.2013.02.005.

97. Kim RJ., Wu E., Rafael A., et al. The use of contrast-enhanced magnetic resonance imaging to identify reversible myocardial dysfunction. N Engl J Med 2000;343(20):1445–53. Doi: 10.1056/NEJM200011163432003.

98. Greenwood JP., Maredia N., Younger JF., et al. Cardiovascular magnetic resonance and single-photon emission computed tomography for diagnosis of coronary heart disease (CE-MARC): A prospective trial. Lancet 2012;379(9814):453–60. Doi: 10.1016/S0140-6736(11)61335-4.

99. Watkins S., McGeoch R., Lyne J., et al. Validation of magnetic resonance myocardial perfusion imaging with fractional flow reserve for the detection of significant coronary heart disease. Circulation 2009;120(22):2207–13. Doi: 10.1161/CIRCULATIONAHA.109.872358.

100. Nagel E., Greenwood JP., McCann GP., et al. Magnetic resonance perfusion or fractional flow reserve in coronary disease. N Engl J Med 2019;380:2418–28. Doi: 10.1056/nejmoa1716734.

101. Sriharan M., McParland P., Harden S., Nicol E. Non-Invasive Coronary Angiography. Coronary Angiography - Advances in Noninvasive Imaging Approach for Evaluation of Coronary Artery Disease. InTech; 2011. p. 99-122. DOI: 10.5772/22475.

Figure legends

Figure 1. Aberrant coronary arteries on coronary CMR angiography. (A) Maximum intensity projection image from a 1D navigator coronary CMR angiography sequence demonstrating an aberrant circumflex artery (black arrowheads) arising from the right coronary artery (RCA) passing between the aorta (Ao) and the right atrium (RA). Note also the resultant artefact (yellow arrowheads) due to cardiac motion. (LA=left atrium). (B) Maximum-intensity projection images of whole-heart coronary CMR angiography acquired with a gradient-echo sequence at 3T and (C) reformatted coronary CTA in a young adult showing anomalous left anterior descending (LAD) coronary artery (arrows) that arises from the proximal segment of the RCA and runs in an inter-arterial course between the aorta (Ao) and main pulmonary artery (PA). Adapted with permission from Sriharan M et al. 2011 (101) and Hamdy A. et al. 2017 (17).

Figure 2. Coronary artery aneurysm on coronary CMR angiography. (A) 6-year-old child with RCA aneurysms secondary to Kawasaki disease. Thin-slab maximum-intensity projection images of the initial whole-heart coronary CMR angiography showed 3 RCA aneurysms. (B) On follow up coronary CMR angiography, all aneurysms showed significant reduction in size and change of morphology. (C and D) Corresponding invasive X-ray coronary angiography shows the same changes. Reproduced with permission from Hamdy A. et al. 2017 (17).

Figure 3. Self-navigated whole-heart coronary CMR angiography. (A–F) Examples of the comparison between multiplanar reformats of the whole-heart self-navigated coronary CMR angiography data sets (top row) and the corresponding X-ray coronary angiograms (bottom row) in three patients. The lesion in the proximal LAD artery and just distal to the take-off of a diagonal branch can clearly be identified in the first patient in (A), confirmed on the X-ray angiogram in (B). The luminal narrowing of the proximal RCA in the second patient on (C) can be identified, the further course of this artery is obscured in the region of a stent. The same inter-stent restenoses can be identified in (D). In the third patient, in (E), significant disease is identified in the proximal LAD and is confirmed on (F), the X-ray coronary angiogram. Arrows = stenoses. Reproduced with permission from Piccini D. et al. 2014 (54).

Figure 4. Whole-heart coronary CMR angiography from three patients using iNAV and d1D navigator. (A, D) 24-year-old male with bicuspid aortic valve, (B, E) 40-year-old male with aortic coarctation, (C, F) 26-year-old male with pulmonary autograft replacement. Arrows highlight coronary segments with improved visualization. Reproduced with permission from Henningsson M. et al. 2016 (60).

Figure 5. Three patients with CAD on coronary CMR angiography. Diagnosis using coronary CMR angiography (top row) and confirmed with invasive X-ray angiography (bottom row). Reproduced with permission from Henningsson M. et al. 2017 (61).

Figure 6. Beat-to-beat and bin-to-bin respiratory motion corrected coronary CMR angiography. (A) Acquisition scheme and beat-to-beat image-navigator based translational motion correction: In each heartbeat, a T2 preparation prepulse (T2p) is applied, followed by the 2D iNAV, a spectral fat saturation pulse, and image acquisition. (B) Reconstruction takes place in two steps. First, (superior-inferior (SI) and left-right (LR) translation of the heart is estimated from the 2D iNAVs. Data are grouped into bins according to the SI respiratory

position, and intra-bin beat-to-beat translational motion (SI and LR) is corrected in k-space for each bin. Each binned dataset is reconstructed with parallel imaging, and the resulting images are registered to a common respiratory position (usually end-expiration) to retrieve the corresponding non-rigid motion fields. The motion fields are used to correct inter-bin nonrigid motion directly within the reconstruction.

Figure 7. Motion corrected and patch-based undersampled reconstructed (PROST) coronary CMR angiography. Acquisition and motion correction is performed with an undersampled 3D variable density spiral-like Cartesian trajectory (VD-CASPR), preceded by 2D image navigators (iNAV), T_2 preparation, and fat saturation pulses. iNAVs are used to estimate and correct for the beat-to-beat 2D respiratory-induced motion of the heart as shown in Figure 6.A. (A) 3D-PROST reconstruction involves 2 stages of an augmented Lagrangian optimization scheme. In stage 1, image reconstruction is performed with patch prior and data consistency enforcement. In stage 2, image denoising is performed using 3D block-matching, which groups similar 3D patches in the image, followed by a low-rank approximation of each group using singular value decomposition shrinkage. The denoised volume from stage 2 is used in the reconstruction process in stage 1 as prior knowledge to regularize the reconstruction problem and further reduce noise. (B) Example of reformatted images of the RCA from 3 representative healthy subjects acquired at 1.2 mm^3 isotropic resolution with a fully sampled free-breathing whole-heart coronary CMR angiography acquisition with 100% respiratory efficiency, and with 2 undersampled acquisitions (Acc×5 and Acc×9), reconstructed using iterative SENSE (itSENSE), conventional compressed-sensing (CS) and 3D-PROST. 3D-PROST provides higher image quality and sharpness (red and yellow arrows) than itSENSE and CS for both acceleration factors, achieving similar image quality to the fully sampled reference. Acquisition times (AT) are expressed as min:s. Adapted with permission from Bustin A et al. 2018 (62).

Figure 8. "Free Running" coronary CMR angiography. Multiplanar reformat of the RCA of a healthy subject which shows the proximal and mid segments (A–C) together with the distal part (D–F) of the coronary artery. Selected reformats obtained from the free-running 4D approach are shown in (A, B, D, E) while the diastolic ECG-triggered respiratory self-navigated dataset is displayed in (C and F). In the left column (A, D), images reconstructed during the systolic rest period are shown adjacent to those reconstructed for the most quiescent diastolic period (B, E). Reproduced with permission from Coppo et al. 2015 (28).

Figure 9. Respiratory-resolved 3D radial coronary CMR angiography with XD-GRASP reconstruction. Sparsity is exploited along the respiratory dimension to remove aliasing artefacts due to undersampling. Examples of multiplanar reformatted coronary arteries from one representative healthy adult subject. Although respiratory self-navigated reconstruction with 1D motion correction could achieve high image quality (top row), a clear improvement in sharpness as well as visible vessel length (arrows) can be noticed in both four respiratory phases (middle row) and six respiratory phase (bottom row) XD-GRASP reconstructions. LCX, Left Circumflex. Reproduced with permission from Piccini D. et al 2017 (74).

Figure 10. Respiratory-resolved 3D Cartesian coronary CMR angiography with XD-ORCCA reconstruction. XD-ORCCA has been proposed to extend XD-GRASP to Cartesian k-space sampling by using translational motion from iNAVs to correct for intra-bin motion and to increase the sparsity in the respiratory direction, by aligning the respiratory resolved images to a common respiratory position. (A) XD-ORCCA achieves consistent high quality for all respiratory phases (3/5 respiratory phases shown from end-expiration to end-

inspiration), being superior to XD-GRASP in terms of image quality, (B) Good agreement between XD-ORCCA and coronary CTA is observed in a patient with CAD. Adapted with permission from Correia T et al. 2018 (78).

Figure 11. Representative case of a suspected CAD patient with a CHIP in the mid LAD on pre-contrast CATCH. (A) Pre-contrast T_1-weighted, anatomical reference and fusion images. (B) coronary CTA, (C) X-ray angiography. (D) OCT cross-sectional image at the corresponding location of the CHIP on CATCH. Arrows point to signal-poor regions, suggesting a large lipid pool. Dotted lines represent the location and orientation of the cross-sectional images at the lesion which are shown in boxes. Reproduced with permission from Xie Y. et al 2017 (92).

Figure 12. **BOOST framework for simultaneous 3D whole-heart non-contrast bright-blood and black-blood CMR for coronary angiography and thrombus visualization.** (A) A T_2Prep-IR module is applied at odd heartbeats to enable coronary lumen visualization with improve contrast between blood and myocardium. A short TI is set to null the signal from epicardial fat. At even heartbeats, data acquisition is T_2 prepared and performed with a high flip angle using spectral pre-saturation for fat suppression. Data acquisition is performed using a 3D Cartesian trajectory with spiral profile order and is segmented over multiple heartbeats (yellow, red, blue) to minimize cardiac motion. A 2D iNAV precedes the 3D data acquisition at each heartbeat and is used to estimate respiratory motion along the superior–inferior and right–left direction for both bright-blood datasets (T_2Prep-IR BOOST and T_2Prep BOOST) independently. The two motion-corrected bright-blood datasets are co-registered and then combined in a PSIR-like reconstruction to generate a 3D whole-heart black-blood dataset (PSIR BOOST). (B) Reformatted coronary depiction in two representative healthy subjects obtained with a conventional T_2-prepared bright-blood coronary CMR angiography acquisition and the proposed BOOST sequence. Quantified contrast to noise ratio (CNR) $_{\text{blood-myocardium}}$ significantly improved with the BOOST approach in comparison to the conventional coronary CMR angiography, thus leading to a higher quantified coronary percentage vessel sharpness for both right and left coronary arteries. Adapted with permission from Ginami G. et al 2018 (93).

Central Illustration. Motion corrected CMRA with shorter and predictable scan time Impact of the proposed motion correction framework consisting of 2D beat-to-beat navigation (image navigator based) and 3D non-rigid (bin-to-bin registration) motion correction reconstruction with patch based regularization (3D-PROST) to enable high acceleration factors (shorter and predictable scan time) in comparison to CTCA. CMRA - coronary CMR angiography; CTCA – computed tomography coronary angiography.

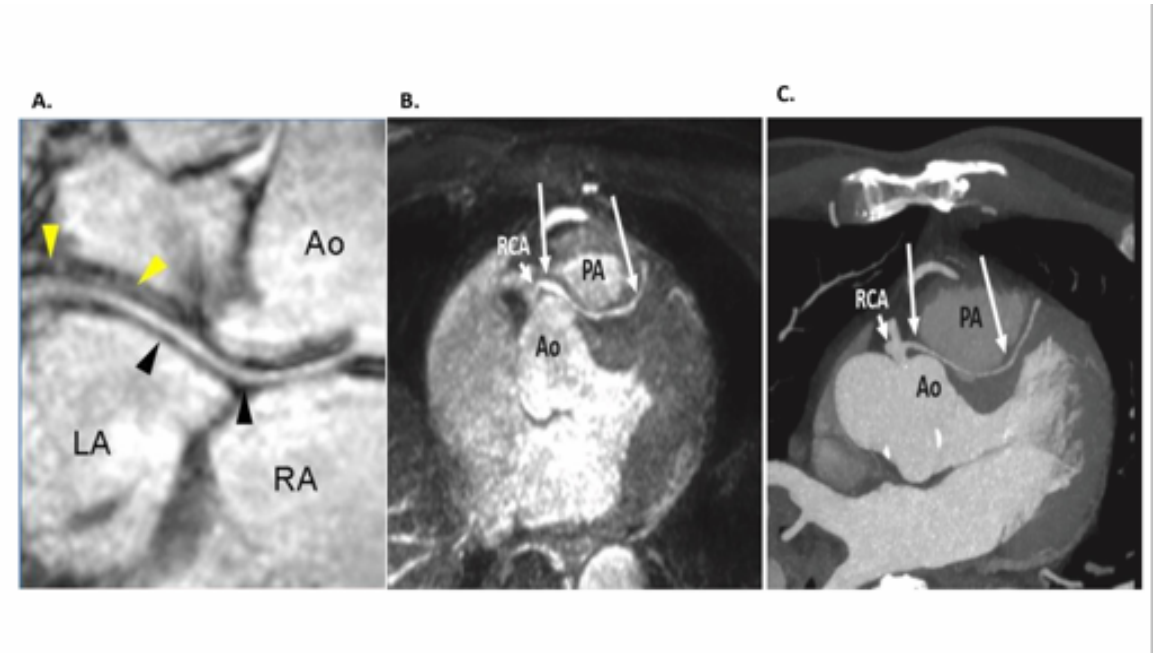
A.
B.
C.
Ao
LA
RA
RCA
PA
Ao
RCA
PA
Ao

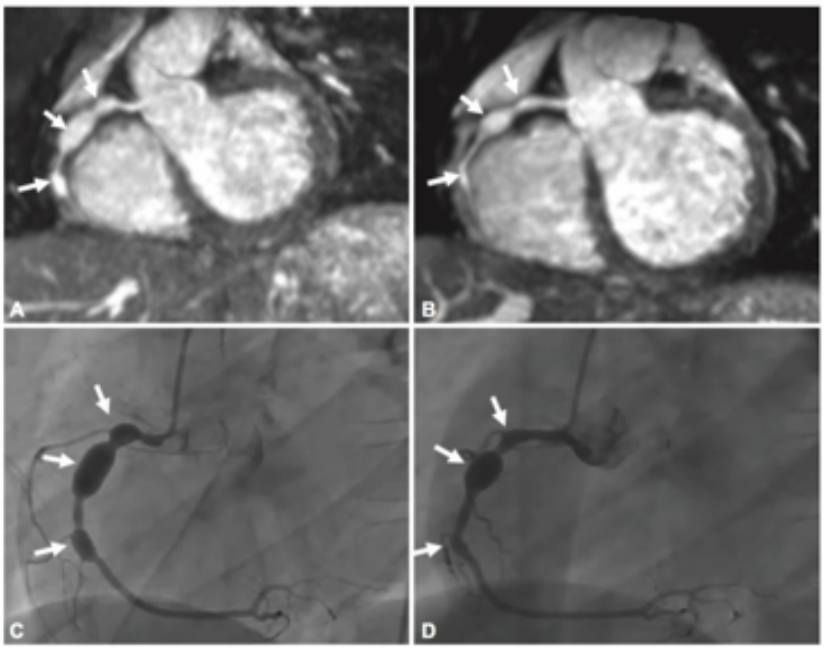
A
B
C
D

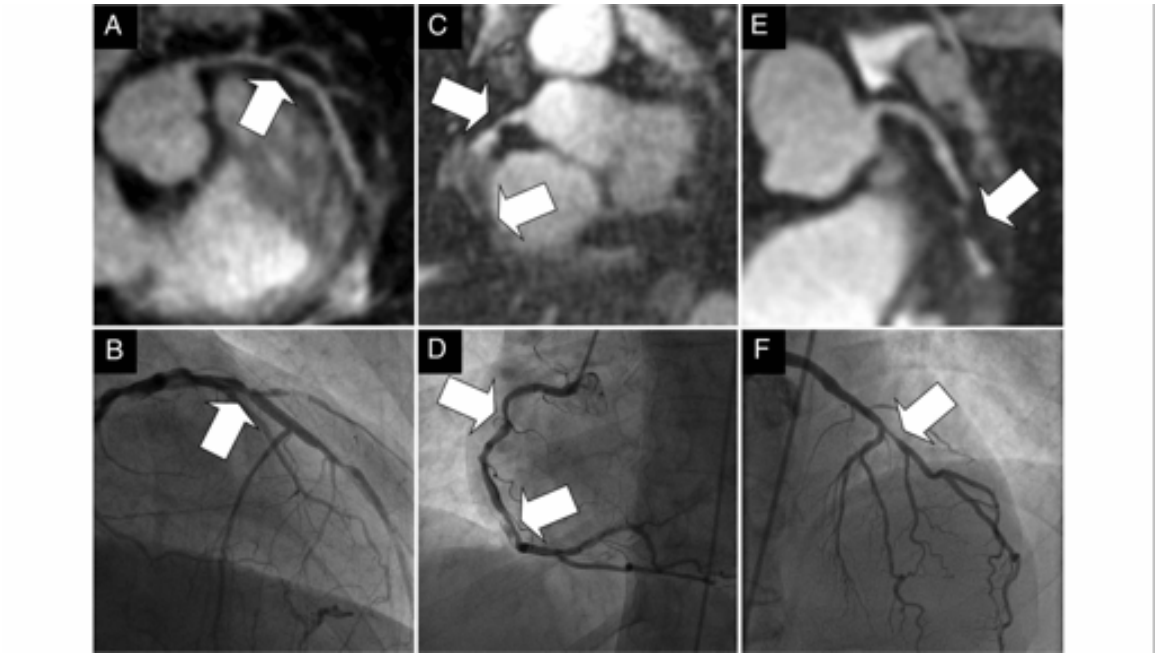
A
C
E
B
D
F

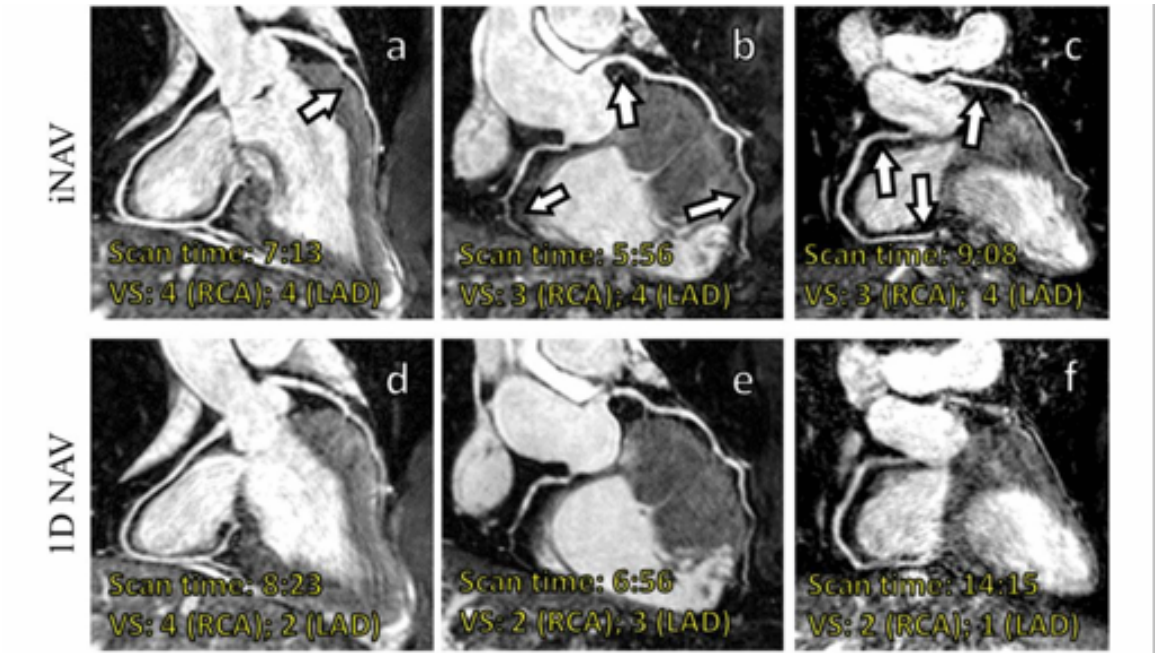
iNAV
1D NAV
a
b
c
d
e
f
Scan time: 7:13
VS: 4 (RCA); 4 (LAD)
Scan time: 5:56
VS: 3 (RCA); 4 (LAD)
Scan time: 9:08
VS: 3 (RCA); 4 (LAD)
Scan time: 8:23
VS: 4 (RCA); 2 (LAD)
Scan time: 6:56
VS: 2 (RCA); 3 (LAD)
Scan time: 14:15
VS: 2 (RCA); 1 (LAD)

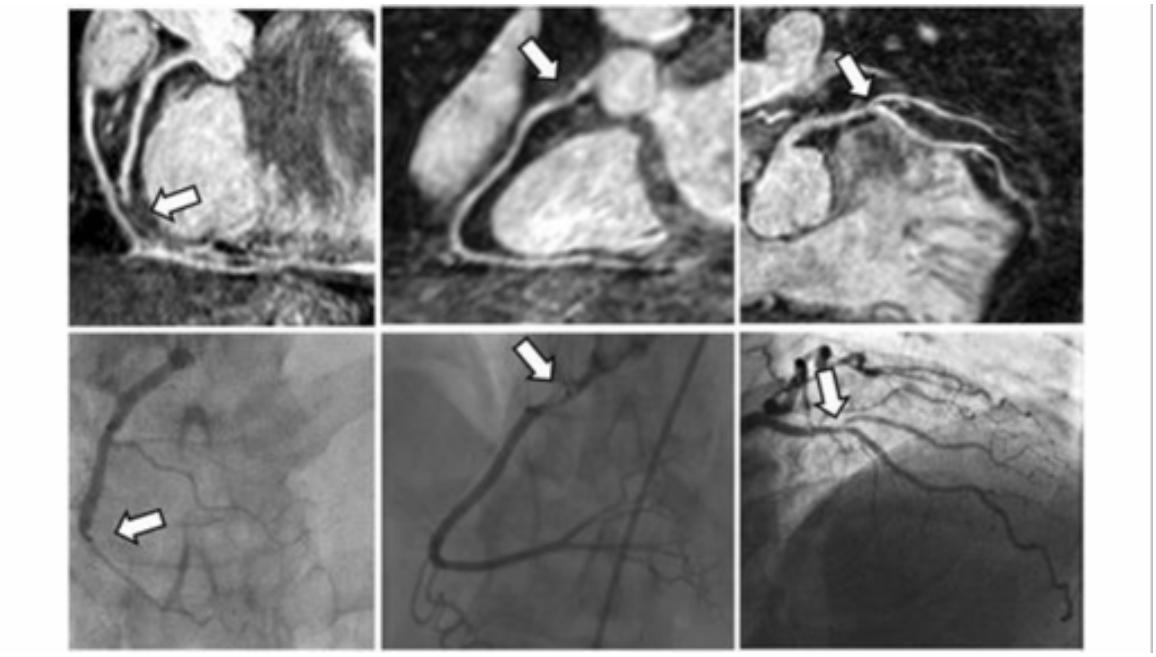

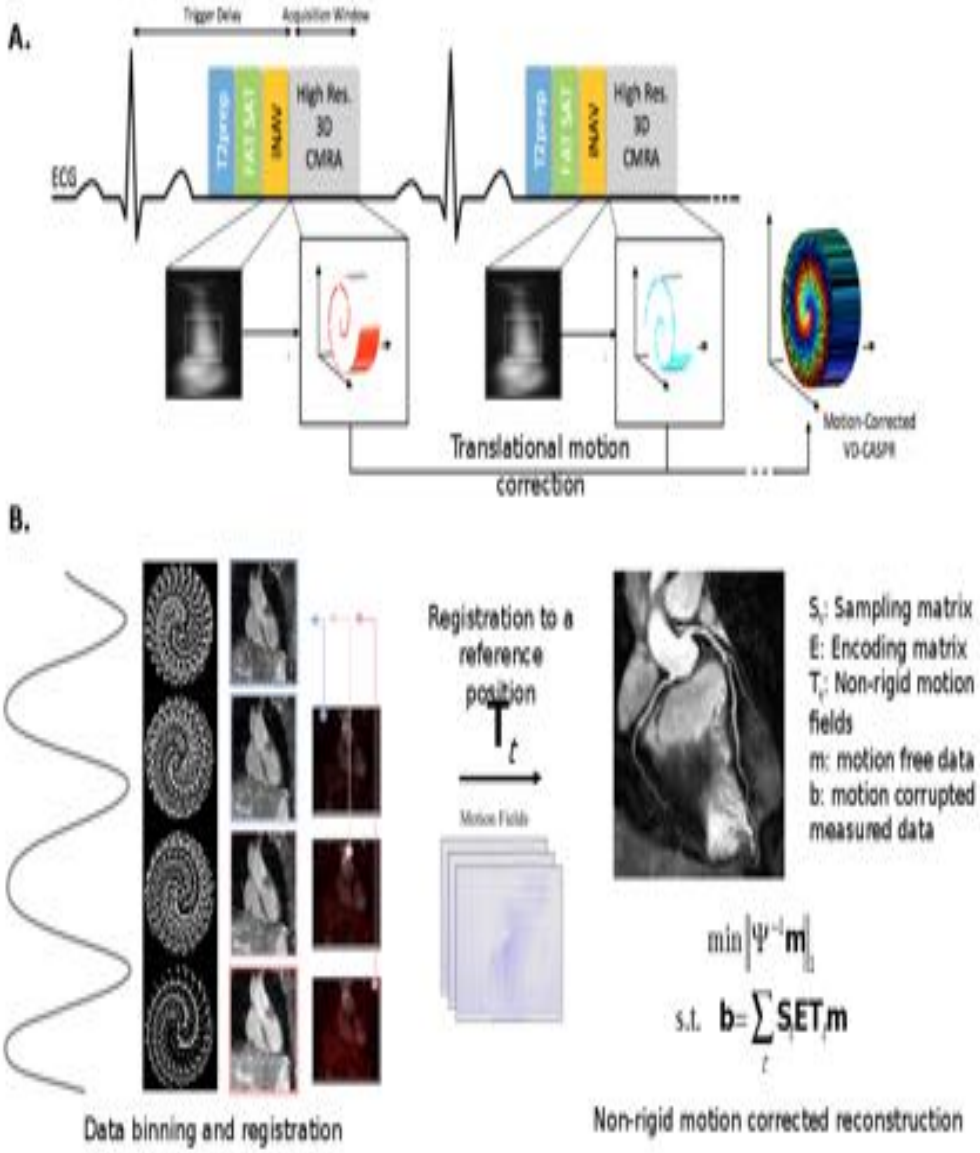
A.
Trigger Delay
Acquisition Window
ECG
T2prep
FAT SAT
iNAV
High Res. 3D CMRA
Translational motion correction
Motion-Corrected VD-CASPR
B.
Registration to a reference position
Motion Fields
S_t: Sampling matrix
E: Encoding matrix
T_t: Non-rigid motion fields
m: motion free data
b: motion corrupted measured data
$\min \|\Psi^{-1}\mathbf{m}\|_1$
s.t. $\mathbf{b} = \sum_t \mathbf{S}\mathbf{E}\mathbf{T}_t\mathbf{m}$
Data binning and registration
Non-rigid motion corrected reconstruction

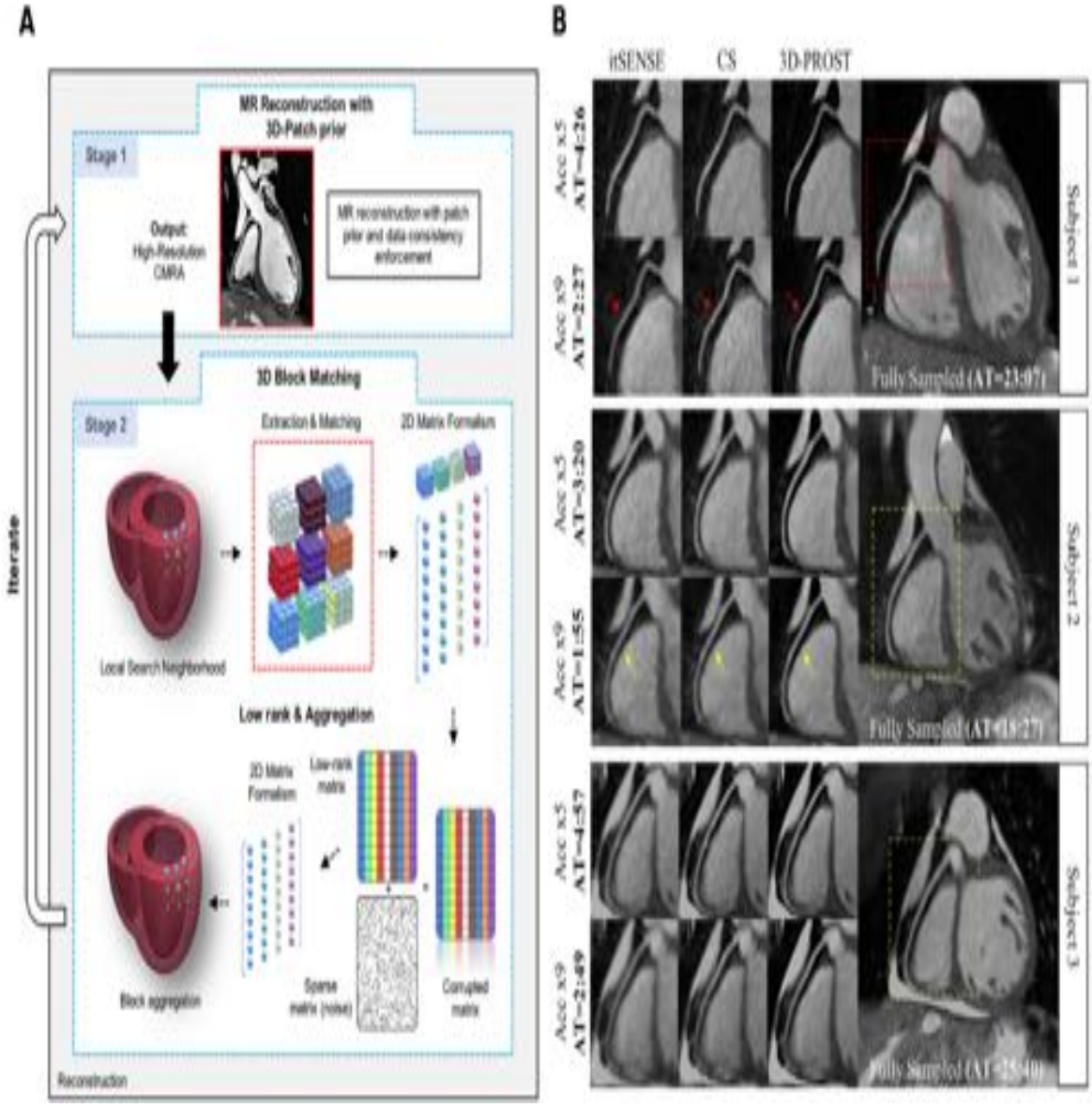
A
MR Reconstruction with 3D-Patch prior
Stage 1
Output: High-Resolution CMRA
MR reconstruction with patch prior and data consistency enforcement
3D Block Matching
Stage 2
Extraction & Matching
2D Matrix Formalism
Local Search Neighborhood
Low rank & Aggregation
2D Matrix Formalism
Low-rank matrix
Sparse matrix (noise)
Corrupted matrix
Block aggregation
Iterate
Reconstruction
B
iSENSE
CS
3D-PROST
Acc x5 AT=4:26
Acc x9 AT=2:27
Fully Sampled (AT=23:07)
Subject 1
Acc x5 AT=3:20
Acc x9 AT=1:55
Fully Sampled (AT=18:27)
Subject 2
Acc x5 AT=4:57
Acc x9 AT=2:49
Fully Sampled (AT=25:40)
Subject 3

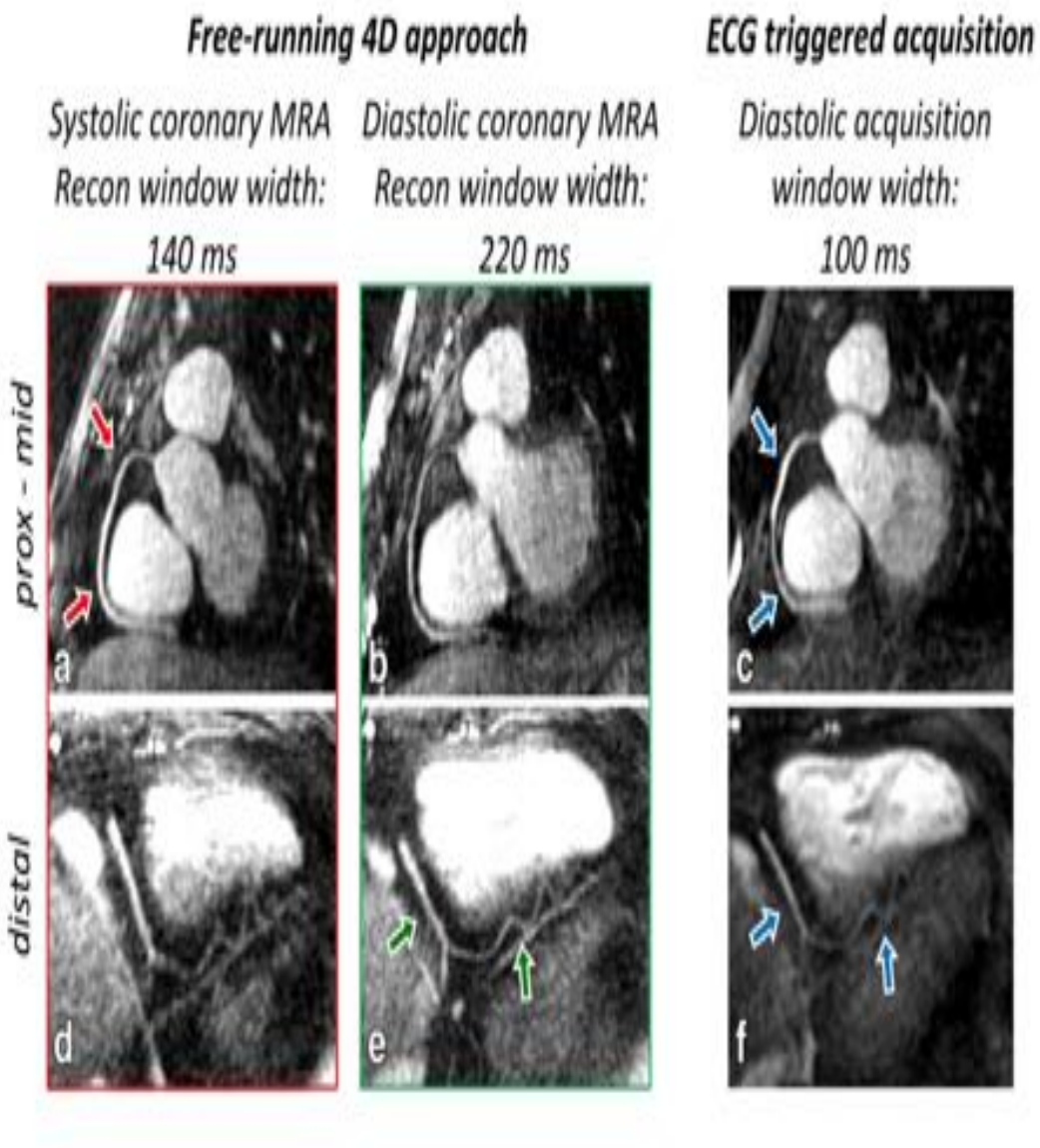
Free-running 4D approach
ECG triggered acquisition
Systolic coronary MRA
Recon window width:
140 ms
Diastolic coronary MRA
Recon window width:
220 ms
Diastolic acquisition
window width:
100 ms
prox - mid
distal
a
b
c
d
e
f

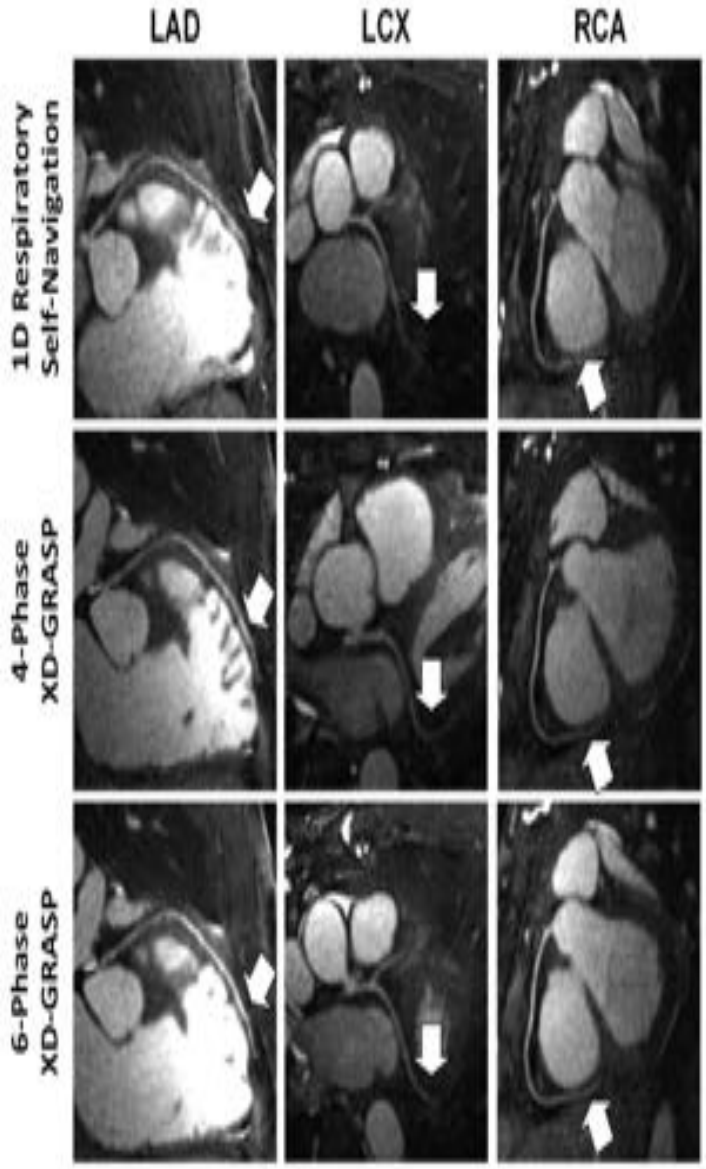
LAD
LCX
RCA
1D Respiratory Self-Navigation
4-Phase XD-GRASP
6-Phase XD-GRASP

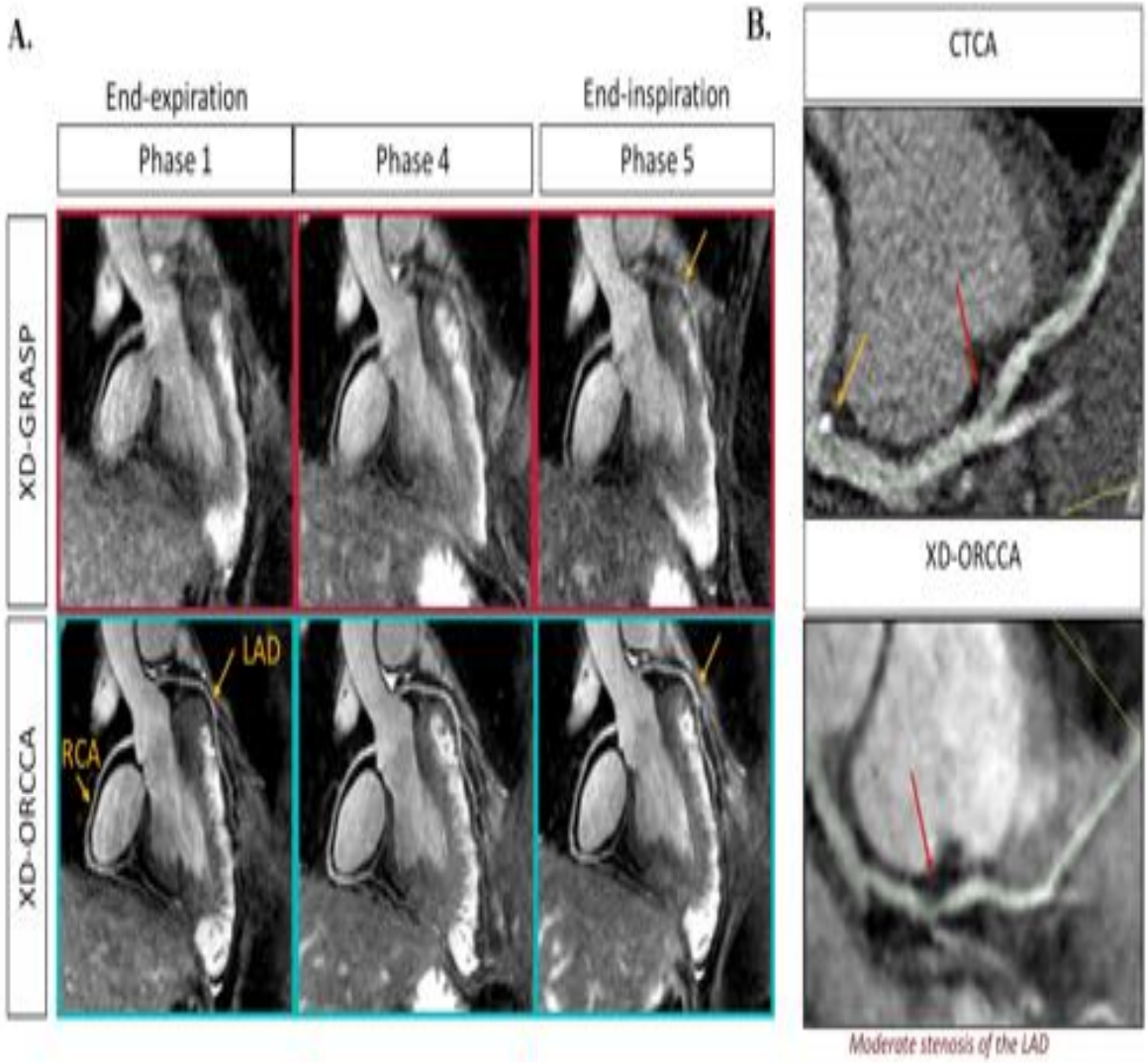
A.
B.
End-expiration
End-inspiration
Phase 1
Phase 4
Phase 5
XD-GRASP
XD-ORCCA
LAD
RCA
CTCA
XD-ORCCA
Moderate stenosis of the LAD

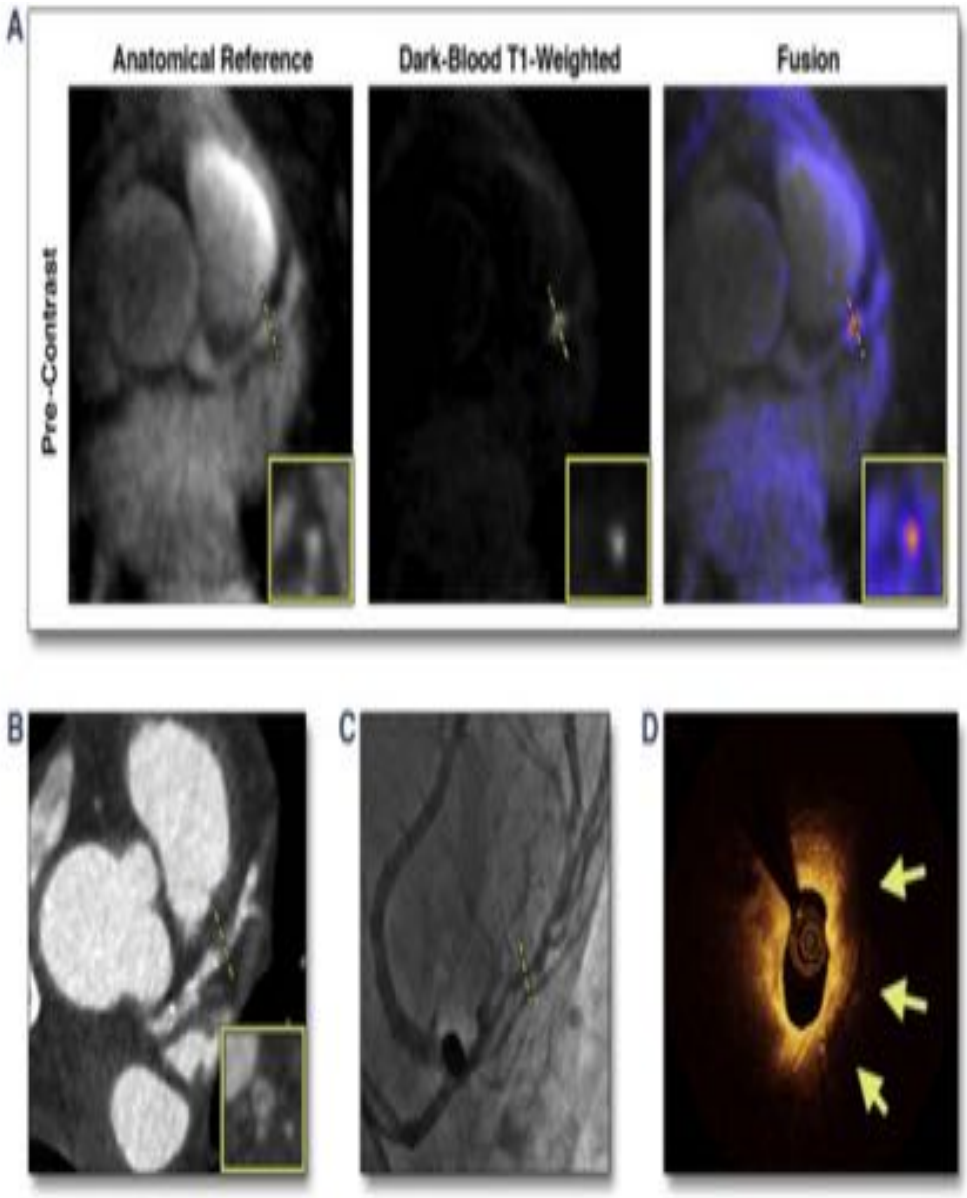
A
Anatomical Reference
Dark-Blood T1-Weighted
Fusion
Pre-Contrast
B
C
D

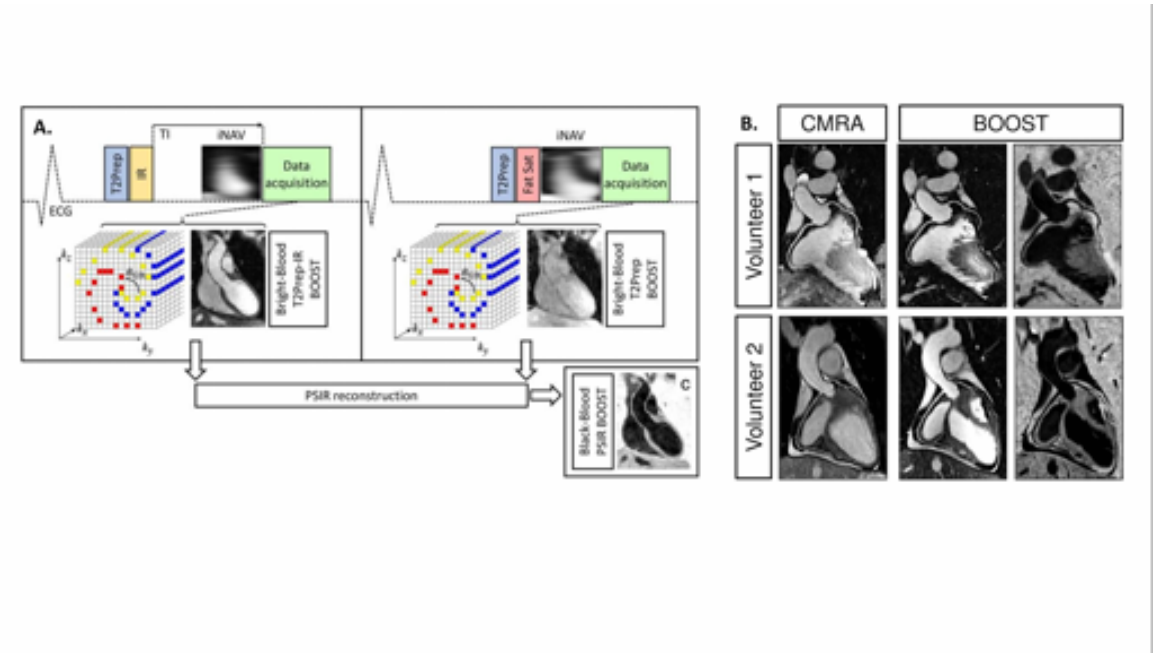
A.
TI
INAV
T2Prep
IR
Data acquisition
ECG
Bright-Blood T2Prep-IR BOOST
INAV
T2Prep
Fat Sat
Data acquisition
Bright-Blood T2Prep BOOST
PSIR reconstruction
Black-Blood PSIR BOOST
B.
CMRA
BOOST
Volunteer 1
Volunteer 2

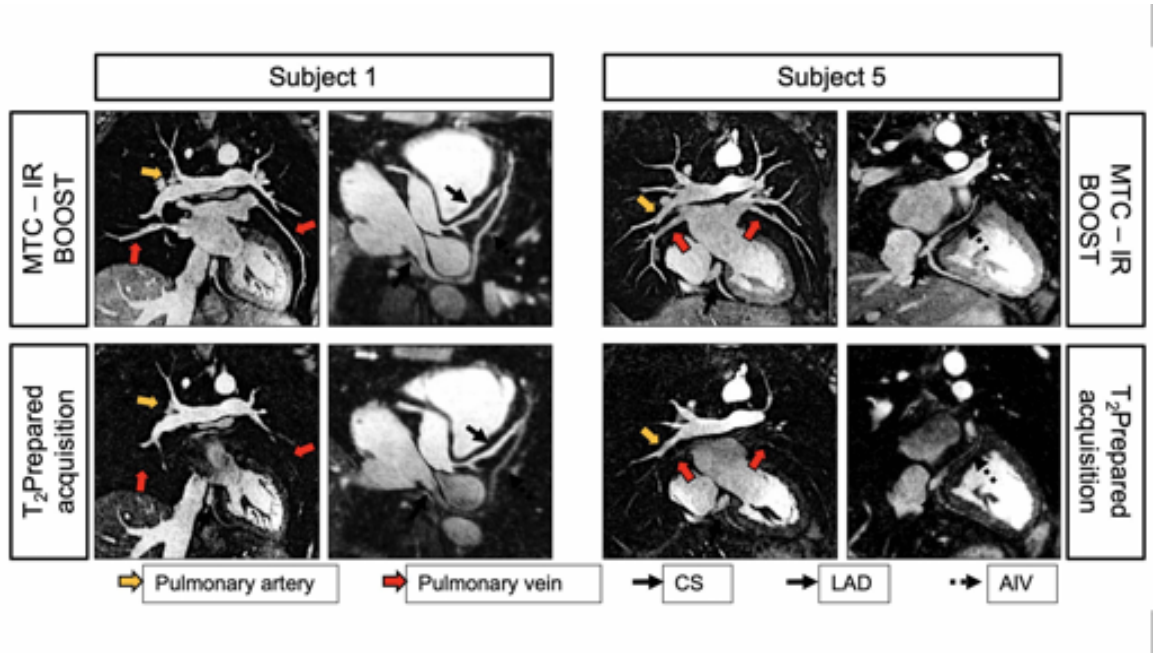
Subject 1
Subject 5
MTC – IR BOOST
T2Prepared acquisition
Pulmonary artery
Pulmonary vein
CS
LAD
AIV

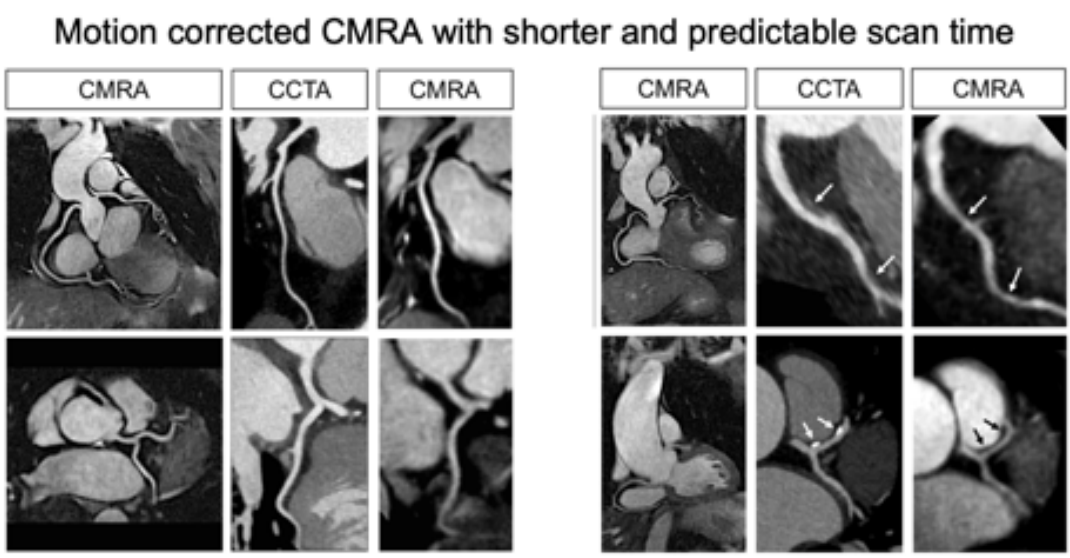

Central illustration: Impact of the proposed motion correction framework consisting of 2D beat-to-beat navigation (image navigator based) and 3D non-rigid (bin-to-bin registration) motion correction reconstruction with patch based regularisation (3D-PROST) to enable high acceleration factors (shorter and predictable scan time) in comparison to CTCA. CMRA - coronary CMR angiography; CTCA – computed tomography coronary angiography.